Numerical Investigation on Propulsion by Undulating Plate

by Zuogang Chen*, Yasuaki Doi**

Summary

Unsteady viscous flow field around an undulating advancing plate in low Reynolds number range is numerically studied. The main objective is to study the abilities of an undulating plate to produce thrust and achieve higher propulsive efficiency in low Reynolds number range. The Reynolds number based on the oncoming velocity and the plate length is 1 000. The flow around an undulating plate is simulated by solving the full 3 D unsteady Navier-Stokes equation in a primitive value formulation. The numerical scheme is based on the MAC method where the Navier-Stokes equation is solved by the time marching method on a body fitted coordinate system.

The simulation shows that pressure is acting as thrusting force while frictional force is acting as resistance during the undulating motion. Strouhal number is the most important governing parameter for the propulsive efficiency. The propulsive efficiency is enhanced with the increase of the Reynolds number. The advancing thrust mainly comes from the aft part of the plate and the modification of the plate shape can improve the propulsive efficiency. The present study is expected to be applied for the development of a propulsor for micro-hydro-machine.

1. Introduction

The flow field around a swimming fish or an aquatic mammal has been investigated for a long time by the researchers in various field of study such as biology, physical science and engineering. This interest has been inspired not only to understand and simulate an efficient swimming propulsion, but also to utilize the results for engineering application. Fast-starting and maneuvering of flexible-hull vehicles can be significantly better than the performance of rigid bodies, because the flow can be controlled over the entire body of the vehicle through the appropriate flexion of the body. Experimental and simulated results[1),2)] demonstrated the ability of flexible-hull vehicle to achieve high maneuverability and turbulence reduction through flow control. Even Barrett et al.[2)] pointed out that the power required to propel an actively swimming, streamlined, fish-like body was significantly smaller than the power needed to tow the body straight and rigid at the same speed. Their parametric investigation showed a sensitivity of drag reduction to the non-dimensional frequency (Strouhal number), the amplitude of body oscillation and wavelength, the angle of attack and the phase angle of the tail fin.

In the field of theoretical hydrodynamics, numerous studies on two and three dimensional flow around a fish-like body have been done since the slender-fish theory of Lighthill[3)] and two dimensional unsteady lifting surface theory of Wu[4)] and have contributed to the present understanding of the hydrodynamic and biological aspects of swimming. Koryenna[5)] quoted the parameter of the moving surface as the ratio of the velocity of the moving surface to the mainstream velocity to discuss the effects of moving surfaces.

Although experiments with flexible-hull vessels and direct flow measurements on live fish are a reliable way to obtain data on maneuvering flexible bodies and to corroborate analytical predictions, the flow is still hard to be studied precisely. Therefore, it is necessary to develop the capability to compute the flow past surfaces in arbitrary motion[6)]. The arbitrary motion can include oscillation and deformation of simple and complex surfaces as well as varying separation between the bodies in response to the varying hydrodynamics interactions. The unsteady viscous flow around an oscillating hydrofoil has been solved by many researchers mainly for a rigid foil by the recent progress of computational fluid dynamics. Liu et al.[7)] analyzed a tadpole propulsion using a three-dimensional computational fluid dynamic model of undulatory locomotion that simulates viscous and unsteady flow around an oscillating body of arbitrary 3 D geometry. Nakaoka and Toda[8)] investigated the flow field around the

* Hiroshima University, Graduate School
** Hiroshima University

Received 10 th July 2000
Read at the Autumn meeting 16, 17 th Nov. 2000

wing (NACA 0010) which moved like a fish by Navier-Stokes solver using moving grid approach. The results showed the fish-like motion was effective to get propulsive force. In that paper, three motion models were compared to each other and meaningful conclusion was drawn to produce a large mean thrust. Kim et al.[9] investigated a peristaltic propulsion in highly viscous fluid, and found that the effective motion of peristaltic propulsion depends on the Reynolds number.

The present paper focuses on the relationship between the propulsive efficiency and Reynolds number, Strouhal number and the shape of the plate through the simulation of unsteady flow around an undulating plate in low Reynolds number range.

2. Modeling of wavy oscillating plate

The simulated undulating body is a rectangular plate with aspect ratio of 1/3, which undulates actively in unbounded oncoming flow, where x, y and z are the stream-wise, the lateral and the vertical coordinates whose origin locates at the leading edge of the plate. All variables are normalized by the plate length L and oncoming velocity U, as well as the time is normalized by L/U. The movement of the waving plate in y direction is given as following,

$$y(x, t)=ax^n \sin[2\pi b(x-Sp\cdot t)] \quad (1)$$

where a is amplitude, $n=1.1, 2\pi b$ is wave number, Sp is phase velocity, t is time, $0\leqq x\leqq Xend(t)$ where $Xend(t)$ is x-coordinate of the trailing edge calculated as follows,

$$\int_0^{Xend(t)} \sqrt{1+\left(\frac{\partial y}{\partial x}\right)^2}\, dx=1.0 \quad (2)$$

Eq. (2) keeps the length of the plate constant during the undulation. The positive phase velocity sends waves from the leading edge toward the trailing edge. Typical loci for different b are shown in Fig. 1. The Reynolds number based on the oncoming velocity and plate length is ranged from 1000 to 2000.

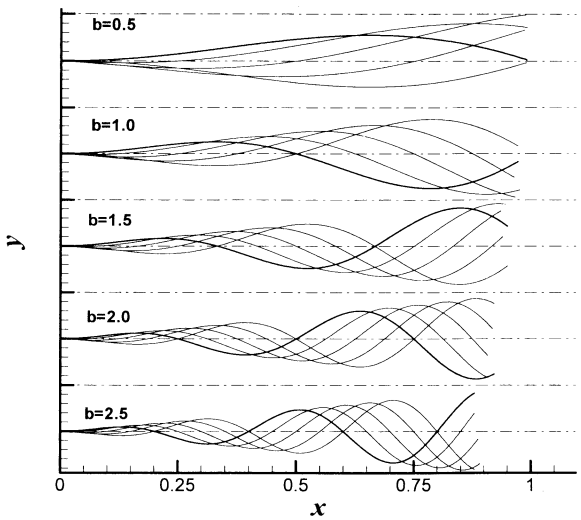

Fig. 1 Vertical-view of the undulating plate for various b (Thick lines: $t=0$, the others: $t=1/8T$, $2/8T$, $3/8T$, $4/8T$ respectively)

3. Numerical scheme

The governing equations are Navier-Stokes equation (3) and continuity equation (4)

$$\frac{\partial \bar{v}}{\partial t}+\bar{v}\cdot\nabla\bar{v}=-\nabla p+\frac{1}{Re}\nabla^2\bar{v} \quad (3)$$

$$\nabla\cdot\bar{v}=0 \quad (4)$$

The full 3 D unsteady Navier-Stokes equation is solved in a primitive value formulation. A numerical co-ordinate transformation is introduced into a body fitted curvilinear co-ordinate system to simplify the computational domain and to facilitate the implementation of boundary conditions. A half H H type grid system is used to simulate the flow around the plate.

The numerical scheme is based on the MAC method where the Navier-Stokes equation is solved by the time marching method on the body fitted coordinate system. The oncoming velocity and the undulating amplitude increase uniformly from zero at $t=0$ to the maximum at $t=1$. After that the oncoming velocity and undulating amplitude keep constant. The first order difference form of the time derivative is used for an explicit advancement in time. The convection terms are discretized by the third order upwind scheme, while all the other spatial derivatives are discretized by the second order central difference scheme. On the body surface, no-slip condition is applied for the velocity. For the pressure, Neumann type condition is applied to satisfy the Navier-Stokes equation. A uniform velocity is applied on the inflow boundary, while a zero-gradient extrapolation is used on the outlet boundary. The Poisson equation for pressure is solved by using SOR (Successive Over Relaxation) method. The validation for the developed code is carried out through the comparison with analytical solution of a flat plate.

The computational domain is $-3.0\leqq x\leqq 5.0$, $-2.0\leqq y\leqq 2.0$, $0\leqq z\leqq 1.0$, where the coordinates are normalized by plate length L. The grid consists of $[124\times 73\times 28]$ points in x, y, z directions where minimum spacing is 0.00526 for $Re=1000$.

4. Computed results and discussions

4.1 Pilot computation for a flat plate

Flow calculation for a flat plate was performed at first. The computation was taken as the basis for the following computation. Table 1 shows the dependence of the computed C_{f1} on $(\Delta y)_{\min}$ for the flat plate at $Re=1000$. C_{f1} represents the integrated frictional drag coefficient along the line $z=1.44\times 10^{-2}$ (which is neighboring to the symmetric line), while C_{fB} represents the frictional drag coefficient by Blasius solution. $(\Delta y)_{\min}$ is minimum grid spacing in y direction.

Table 1 shows the results for rectangle plate with aspect ratio of 1.8. It seems that C_{f1} can approach to

Table 1 Dependence of the computed C_{f1} on $(\Delta y)_{min}$

$(\Delta y)_{min}$	C_{f1}	$(C_{f1}-C_{fB})/C_{fB}$
Blasius Solution	0.0840	----------
0.00847	0.0773	-7.93%
0.00669	0.0809	-3.63%
0.00526	0.0838	-0.27%

Blasius solution (C_{fB}) if $(\Delta y)_{min}$ is chosen carefully. Therefore $(\Delta y)_{min}=0.00526$ was adopted for the calculations at $Re=1000$.

4.2 Choice of the parameters

In order to sound the parameters of undulating motion in eq. (1), the study of live fish swimming was surveyed. The parameters converted from Koryenna's study[5] were shown in Table 2. In inviscid flow, the optimum Sp is estimated to be 1.0, but in viscous flow, Sp is greater than 1.0 in a small degree as shown in Table 2. According to Table 2, the main parameters in this paper were set around that $a=0.1$ and $b=1.5$. As to the aspect ratio of the plate, 1/3 was set in the present study.

Table 2 Parameters chosen by water animals

Water animal varictics	Re	b	Sp	a
Tursiops truneadus	6.0×10^6	1.4	1.33	0.06
Belone	4.5×10^5	2.2	1.15	0.06
Pomatomus saltatrix	6.5×10^5	1.1	1.13	0.12
Sarda sarda	1.6×10^5	1.2	1.12	0.13
Cristivomer namaycush	2.5×10^5	1.4	1.11	0.10

4.3 Self-propulsion condition

The total force acting on the plate varies during the undulating motion. Therefore, in the present study, self-propulsion is defined as the condition where the time-averaged total force becomes zero. The phase velocity Sp is tuned to find the self-propulsion condition. The related parameters are as follows,

$$\bar{C}_{Fx}=\frac{\frac{\int_0^T F_{xf}dt}{T}}{\frac{1}{2}\rho U^2 S},\quad \bar{C}_{px}=\frac{\frac{\int_0^T F_{xp}dt}{T}}{\frac{1}{2}\rho U^2 S} \tag{5}$$

$$\bar{C}_{Tx}=\bar{C}_{Fx}+\bar{C}_{Px} \tag{6}$$

$$C_{Fx}=\frac{F_{xf}}{\frac{1}{2}\rho U^2 S},\quad C_{Px}=\frac{F_{xp}}{\frac{1}{2}\rho U^2 S} \tag{7}$$

$$\eta_P=\frac{\int_T outputdt/T}{\int_T inputdt/T}=\frac{U\cdot\int_T Ddt}{\int_T\left[\int_{\pm S}(\tau_x+p_x)\cdot uds+\int_{\pm S}(\tau_y+p_y)\cdot vds\right]dt} \tag{8}$$

where F_{xf} is x-component of frictional force exerted on the plate, F_{xp} is x-component force by pressure exerted on the plate, T is the period of the undulation, ρ is the density of the fluid, U is the oncoming velocity, S is the area of the plate. The negative symbol of pressure component F_{xp} (against to x-axis) represents thrust and the positive symbol of frictional force component F_{xf} (same to x-axis) represents resistance. When the self-propulsion condition is achieved, the time-averaged total force exerted on the plate becomes zero. Thus the propulsive efficiency η_P is defined by eq. (8) in the present study. The output work rate is the product of the resistance D of a flat plate (computed frictional drag at the same Reynolds number) and the oncoming velocity U. The input work rate is the work rate exerted on the plate to produce the undulation. In eq. (8), τ_x, p_x, τ_y, p_y are x or y-component of frictional stress or pressure exerted on the plate, u and v are x or y-component of the velocity on the plate, $\pm S$ indicates the both sides area of the plate.

Computed results for the case of $Re=1000$, $a=0.1$, $b=1.5$, $n=1.1$ are shown in Table 3. When the phase velocity $S_P=1.56$, $\bar{C}_{Tx}$ is slightly greater than zero, while $S_P=1.57$, $\bar{C}_{Tx}$ is slightly smaller than zero. With the increase of S_P, the frictional force component $\bar{C}_{Fx}$ increases slightly while the pressure component $|\bar{C}_{Px}|$ increases sensitively. $|\bar{C}_{Tx}/\bar{C}_{Fx}|$ is an index to evaluate an error of the self-propulsion condition. From Table 3, it can be seen that η_P has the error less than 1%. More accurate η_P can be obtained by a linear interpolation from the computed results, for example, when $S_P=1.5658$, η_P is interpolated as 0.56843 while the simulated η_P is 0.56846. In order to find a suitable S_P and corresponding η_P, this kind of the linear interpolation can be reasonably used for the further research.

Table 3 Sensitivity of η_P to $\bar{C}_{Tx}/|\bar{C}_{Fx}|$

Re=1000, a=0.1, b=1.5, n=1.1

Sp	$\bar{C}_{Fx}$	$\bar{C}_{Px}$	$\bar{C}_{Tx}$	$\bar{C}_{Tx}/\lvert\bar{C}_{Fx}\rvert$	η_P
1.56	0.1300	-0.1288	0.12×10^{-2}	0.90%	0.576
1.57	0.1305	-0.1313	-0.8×10^{-3}	-0.63%	0.563
1.5658	0.1303	-0.1303	0.2×10^{-4}	0.018%	0.568

Fig. 2 shows the simulated history of hydraulic force coefficients (C_{Fx}, C_{Px}), which are x-components of frictional and pressure force given by eq. (7). In Fig. 2 $Yend$ indicates the position of the trailing edge in y-direction. It is found that the amplitude of C_{Fx} is smaller than that of C_{Px}. The motion of plate at the ordinate is sinusoidal, however C_{Fx} does not oscillate in the sinusoidal motion. The resultant force ($C_{Fx}+C_{Px}$) oscillates around zero. Because of the symmetry of the plate movement, there are two crests and troughs within one period of undulating motion. Fig. 3 shows pressure distributions on the symmetric plane ($z=0$) when the thrust reaches the maximum (C_{Px} reaches the minimum at $t=2.604$) and when the thrust reaches the minimum (C_{Px} reaches the maximum at $t=2.707$). When the thrust reaches the maximum, there are two zones where the pressure acting on both side of plate

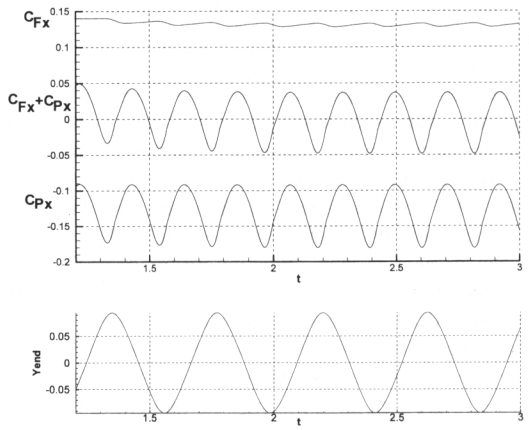

Fig. 2 Simulated time history of hydraulic force coefficients (the upper) and the corresponding position of the trailing edge in y-direction (the lower) for $Re=1\,000$, $a=0.1$, $b=1.5$, $Sp=1.5658$

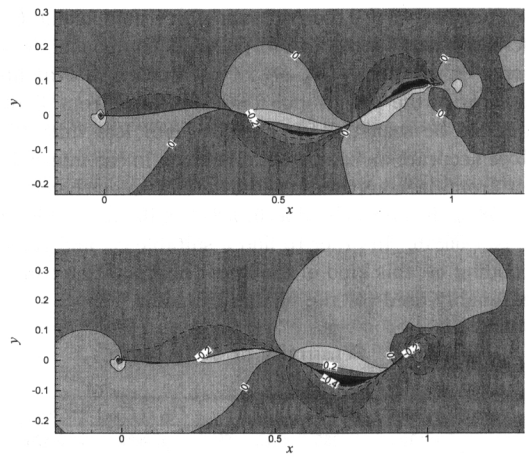

Fig. 3 Pressure contours at symmetric plane when thrust reaches maximum (the upper) and the minimum (the lower) for $Re=1\,000$, $a=0.1$, $b=1.5$, $Sp=1.5658$ (Solid lines: positive, dashed lines: negative, interval: 0.1)

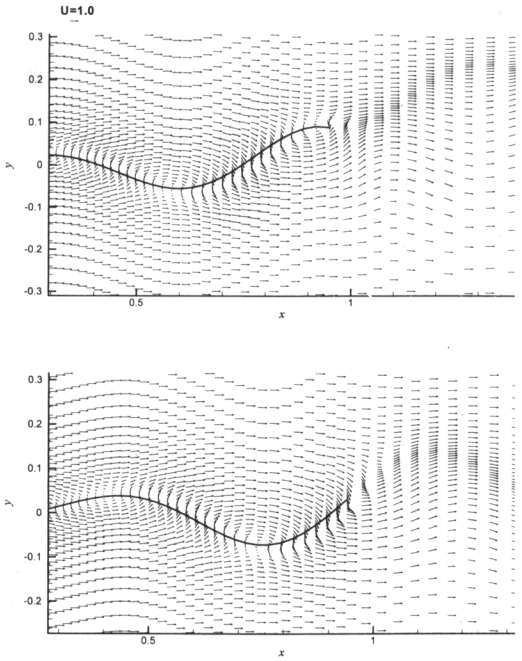

Fig. 4 Velocity distributions on symmetric plane when thrust reaches the maximum (the upper) and the minimum (the lower) for the case of $Re=1\,000$, $a=0.1$, $b=1.5$, $Sp=1.5658$

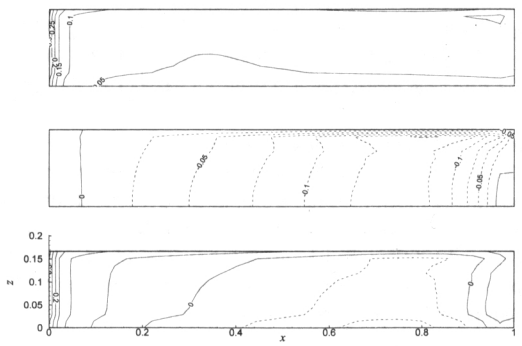

Fig. 5 Distributions of time-averaged x-components of frictional stress (the upper), pressure (the middle) and resultant stress (the lower) for the case of $Re=1\,000$, $a=0.1$, $b=1.5$, $Sp=1.5658$

generates thrust. When the thrust reaches the minimum, there is only one zone where thrust is generated. Fig. 4 respectively show velocity distributions (u-v) on the symmetric plane ($z=0$) at the same time instant. As shown in Fig. 4, the generation of vortex, which is thought to be meaningful for thrust force, is due to a great extent to the plate motion. The velocity in wake behind the plate is higher when the thrust reaches maximum. Fig. 5 shows time-averaged distributions of x-components of frictional stress τ_x, pressure p_x and their resultant force. The frictional stress acts as a resisting force on the whole area of plate, while the pressure acts as a thrusting force. The thrust mainly comes from the aft part of the plate. Figs. 6 and 7 show x-components of frictional force and pressure contours at $t=2.767$ ($0.5T$), 2.821 ($0.625T$), 2.874 ($0.75T$) and 2.927 ($0.875T$) respectively. $0.5T$ indicates the phase is a half of the period. It can be seen that there are two larger pressure gradient zones, one is thrust (negative zone) and the other is resistance (positive zone), which move from the middle to the tail periodically. While,

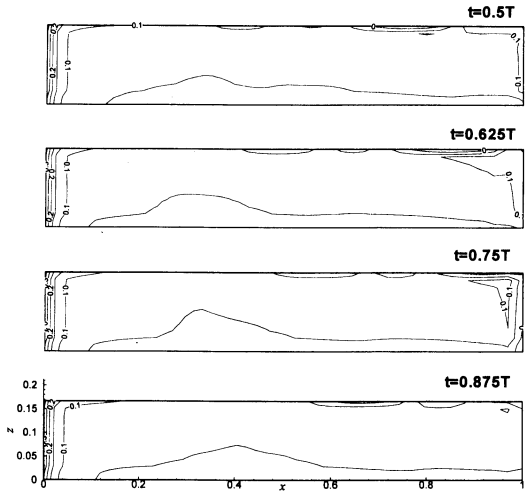

Fig. 6 Distributions of time-averaged x-components of frictional stress at every $0.125T$ step for the case of $Re=1\,000$, $a=0.1$, $b=1.5$, $Sp=1.5658$
(Interval of contour lines: 0.05)

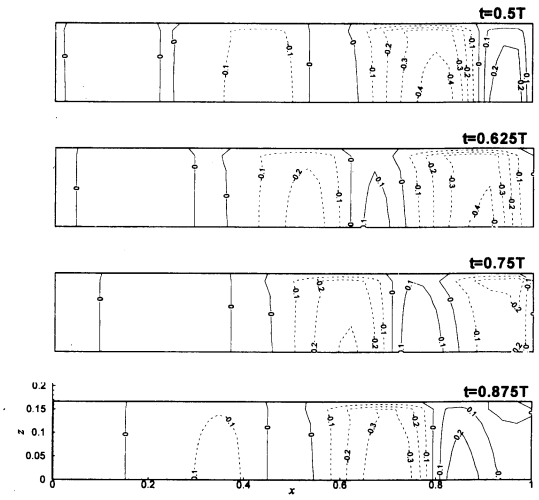

Fig. 7 Distributions of time-averaged x-components of pressure at every $0.125T$ step for the case of $Re=1\,000$, $a=0.1$, $b=1.5$, $Sp=1.5658$
(Interval of contour lines: 0.1)

the distribution of frictional stress does not vary so much during the undulation of the plate.

4.4 Dependence of wave number and amplitude

Dependence of self-propulsion on wave number was investigated. Table 4 shows the calculated self-propulsion condition at $Re=1\,000$, $a=0.1$, $n=1.1$. In Table 4, A is the maximum lateral excursion of the trailing edge of the plate and St is strouhal number, defined by

$$St=f\times A/U \qquad (9)$$

where $f=b\times Sp$ is the frequency of undulation and U is the oncoming velocity. As shown in Table 4, Sp decreases when b increases to get self-propulsion. Fig. 8 shows that the frictional force depends on the wave number. As b becomes larger, the frictional force increases. On the other hand, when b is so small ($b=0.5$) that Sp increases so fast that the frictional force becomes larger. The time-averaged x-component of frictional stress for various b are compared in Fig. 9. It can be seen that the increase comes from the aft of the plate, where the larger frictional force zone enlarges with the increase of b, as well as the smaller frictional force zone decreases. Fig. 10 shows time-averaged x-directional pressure distribution for various b. It is interesting that the patterns of the x-directional pressure distributions are similar, although their wave numbers are different. The peak of the distribution which contributes to produce thrust locates around $0.7\leqq x\leqq 0.8$ for each wave number, while the end of the plate does not contribute to produce thrusting force.

The calculations for $a=0.06$, 0.08, 0.12 or 0.14 respectively were carried out. Fig. 11 shows the relationship between a, b and Sp when self-propulsion is achieved. As increase of a or b, Sp decreases but it is greater than 1. Figs. 12 and 13 show the dependence of propulsive efficiency on a and b. It can be seen that there exists a zone, in which η_P can be beyond 0.55, and that η_P decreases gradually when the values of a and b move away from the zone.

From Figs. 11, 12 and 13, it can be observed that η_P

Table 4 Computed results for self-propulsion at $Re=1\,000$, $a=0.1$

b	Sp	A	St	$\bar{C}_{Fx}$	η_P
0.5	3.10	0.0988	0.153	0.126	0.369
1.0	1.89	0.0967	0.183	0.125	0.524
1.5	1.57	0.0938	0.220	0.130	0.568
2.0	1.41	0.0906	0.256	0.137	0.558
2.5	1.32	0.0875	0.289	0.143	0.524

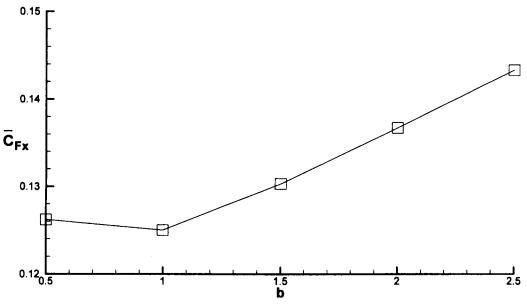

Fig. 8 Dependence of $\bar{C}_{Fx}$ on b
($Re=1\,000$, $a=0.1$)

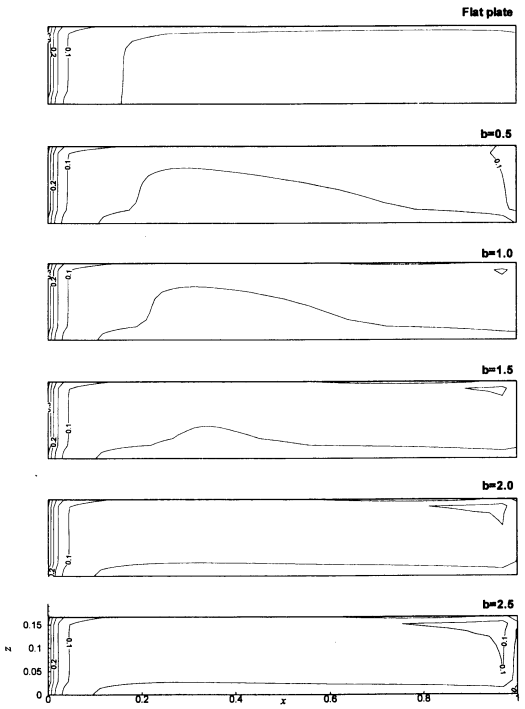

Fig. 9 Time-averaged x-components of frictional stress for various b at $Re=1\,000$, $a=0.1$ (Interval of contour lines: 0.05)

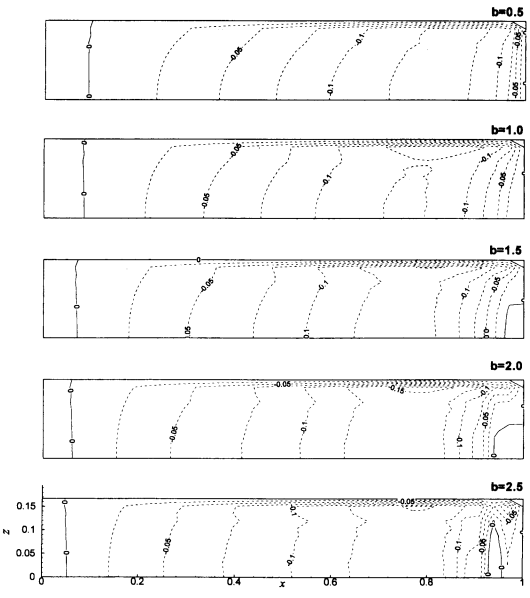

Fig. 10 Time-averaged x-components of pressure for various b at $Re=1\,000$, $a=0.1$ (Interval of contour lines: 0.025)

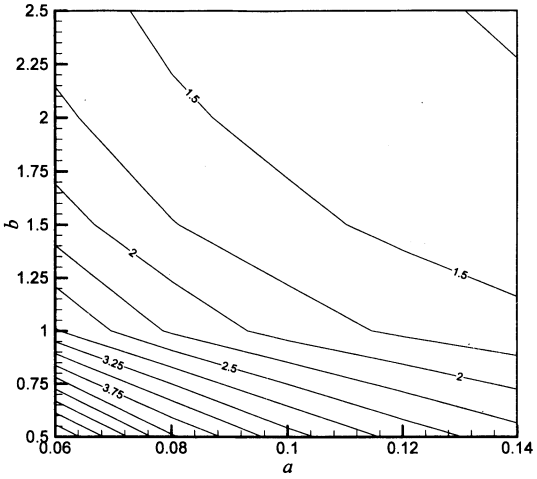

Fig. 11 Dependence of Sp on a and b

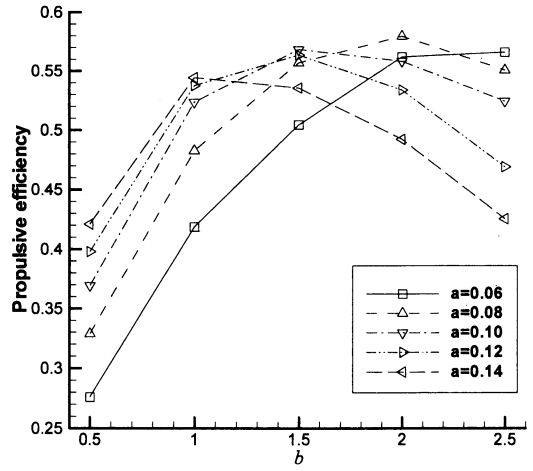

Fig. 12 Dependence of propulsive efficiency on b

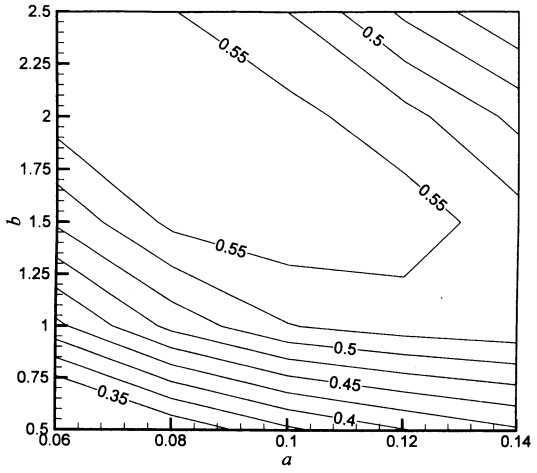

Fig. 13 Contours of propulsive efficiency

seems to depend on a, b and Sp. As shown in eq. (9), these three parameters are combined in one parameter, St (Strouhal number). Fig. 14 shows the dependence of the propulsive efficiency η_P on Strouhal number St. It is obvious that, for an undulating plate, the governing parameter for the propulsive efficiency is not the amplitude, wave number or phase velocity, but Strouhal number. The highest η_P is about 0.58 when St is around 0.23. The higher η_P, which is greater than 0.55 for example, is achieved between $0.2 \leqq St \leqq 0.26$ when Reynolds number is 1 000.

4.5 Dependence on Reynolds number

The effect of Reynolds number on the propulsive efficiency was investigated. Table 5 shows computed results for $Re=2\,000$. Since the main governing parameter is Strouhal number, the computations was carried out for $a=0.1$ with variation of b to test the dependency of propulsive efficiency on Reynolds number. The minimum grid spacing in y-direction, $(\Delta y)_{\min}=0.00323$ was adopted for the calculations of $Re=2\,000$.

Fig. 15 compares the calculated propulsive efficiency. It is found that the peak of η_P for $Re=2\,000$ shifts to the low Strouhal number range. With the increase of

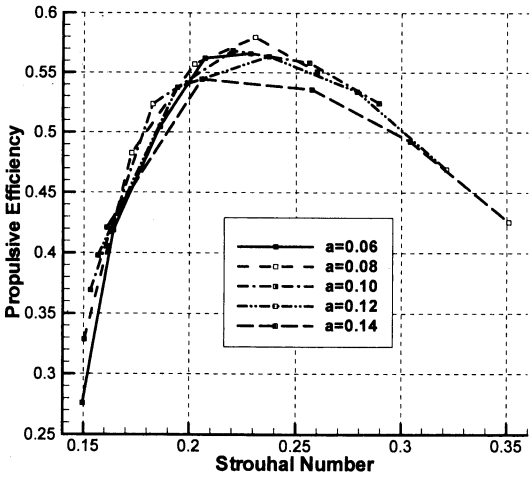

Fig. 14 Dependence of propulsive efficiency on Strouhal Number

Table 5 Relationship between the propulsive efficiency and Strouhal number for $Re=2\,000$

b	Sp	A	St	η_P
0.5	2.67	0.0988	0.132	0.400
1.0	1.69	0.0967	0.164	0.555
1.5	1.44	0.0938	0.203	0.590
2.0	1.32	0.0906	0.240	0.577
2.5	1.27	0.0875	0.277	0.529

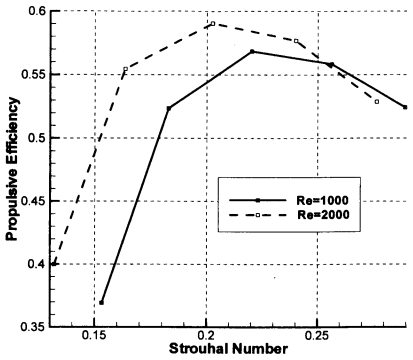

Fig. 15 Effect on propulsive efficiency by Reynolds number ($a=0.1$)

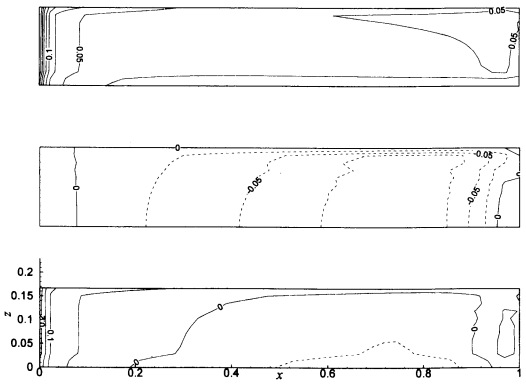

Fig. 16 Distributions of time-averaged force on the plate for $Re=2\,000$, $a=0.1$, $b=1.5$, $Sp=1.44$ (From the top to the bottom: x-components of frictional stress, pressure and resultant force)

Reynolds number, the optimum St decreases (also see Table 2) and the peak value of propulsive efficiency increases. Fig. 16 shows time-averaged distribution of x-component of frictional stress, pressure and their resultant force for the case of $Re=2\,000$, $a=0.1$, $b=1.5$, $Sp=1.44$. The corresponding figure for $Re=1\,000$ is Fig. 5. From those two figures, it is found that the increase of Reynolds number decreases the frictional force but increases the area of zero thrust pressure zone near the tail.

4.6 Trapezoidal profile

From Figs. 3, 5 and 7, the advancing thrust by the undulation mainly comes from the aft part of the plate, which implies the modification of plate profile may enhance the propulsive efficiency. A trapezoidal profile as shown in Fig. 18 is introduced. The ratio of the breadth of bow and aft is 0.5 and the area and the length of plate are same as those of the rectangle plate. Fig. 17 shows some computed results for $Re=1\,000$. The curve of η_P of the trapezoidal plate moves to the

lower strouhal number and the peak value of η_P is larger than the η_P for the rectangle at the same Reynolds number. Therefore, the propulsive efficiency can be enhanced when the profile of the plate is suitably modified. Fig. 18 shows time-averaged distributions of x-components of frictional stress, pressure and their resultant force for the case of $Re=1\,000$, $a=0.1$, $b=1.5$, $Sp=1.51$. When it is compared with Fig. 5, it is found that contour line of pressure less than -0.01 shifts to the tail when the profile of the plate is changed into a trapezoid. That kind of shift can take advantage of the larger area of the trapezoid.

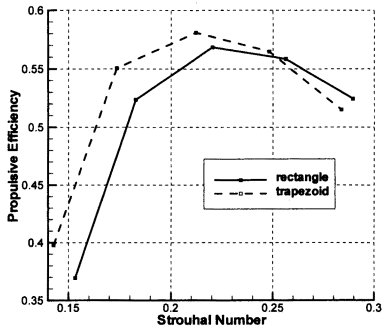

Fig. 17 Comparison of propulsive efficiency at $Re=1\,000$ and $a=0.1$

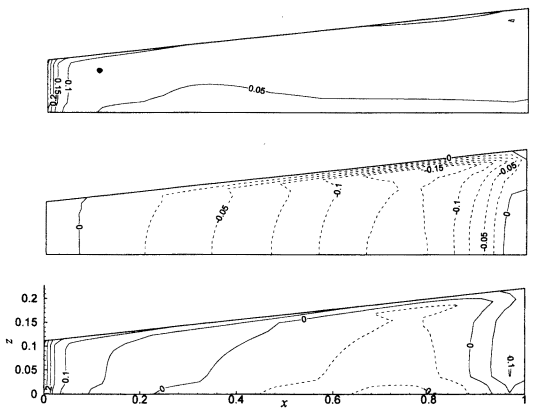

Fig. 18 Distributions of time-averaged force for a trapezoidal profile plate at $Re=1\,000$, $a=0.1$, $b=1.5$, $Sp=1.51$ (From the top to the bottom : x-components of frictional stress, pressure and resultant force)

5. Concluding remarks

The propulsion of the undulating advancing plate in highly viscous fluid is numerically investigated. The numerical simulation shows that the pressure on the plate is acting as thrusting force while the frictional force is acting as resistance during the undulation. The time-averaged distributions of the thrust component of pressure have a similar pattern, even though the wave numbers of undulation are different. The thrusting force is mainly generated near the aft part of the plate, but not at the end of the plate. Strouhal number is the governing parameter for the propulsive efficiency. The optimum propulsive efficiency is enhanced and shifted to low Strouhal number range with the increase of the Reynolds number. The present study is expected to be applied for the development of a propulsor for micro-hydro-machine.

Reference

1) Techet, A. H., Zhang, X., Wolfgang, M. J., Kumph, J. M., Hover, F. S., Yue, D. K. P., Triantafyllou, M. S., Anderson, E. J., McGillis, W. R., Grosenbaugh, M. A., "Flow Control of Flexible-Hull Vehicles", Proceedings of the Eleventh International Symposium on Unmanned Untethered Submersible Technology, 1999, pp. 162-171.
2) Barrett, D. S., Triantafyllou, M. S., Yue, D. K. P., Grosenbaugh, M. A., Wolfgang, M. J., "Drag Reduction in Fish-Like Locomotion", J. Fluid Mech. 1999, Vol. 392, pp. 183-212.
3) Lighthill, M. J., "Note on the Swimming of Slender Fish", J. Fluid Mech., 1960, Vol. 9, pp. 305-317.
4) Wu, T. Y., "Swimming of Waving plate", J. Fluid Mech., 1961, Vol. 10, pp. 321-344.
5) Koryenna L., "Boundary Layer Control at Wave-Like Swimming", Proc. of the International Symposium on Seawater Drag Reduction, 1998, pp. 257-261.
6) Sandberg, W. C., Ramamurti, R., "Unsteady Flow Computations for Oscillating Fins: A Status Report", Proceedings of the Eleventh International Symposium on Unmanned Untethered Submersible Technology, 1999, pp. 182-194.
7) Liu, H., Wassersug, R., Kawachi, K., "The Three-Dimensional Hydrodynamics of Tadpole Locomotion", The J. of Experimental Biology 200, 1997, pp. 2807-2819.
8) Nakaoka, T., Toda, Y., "Laminar Flow Computation of Fish-Like Motion Wing", Proceeding of the Fourth International Offshore and Polar Engineering Conference, 1994, pp. 530-538.
9) Kim, M. C., Mori, K., Doi, Y., Xu, Q., "A Numerical Study on Propulsive Force by Contractive and Dilative Motion in Highly Viscous Fluid", J. of the Society of Naval Architects of Japan, 1998, Vol. 183, pp. 27-33.